Injectivity of Multiple Slugs in Surfactant Alternating Gas Foam EOR
A CT Scan Study

Gong, Jiakun; Vincent-Bonnieu, Sebastien; Kamarul Bahrim, Ridhwan Z.; Mamat, Che A.N.B.; Tewari, Raj D.; Mahamad Amir, Mohammad I.; Groenenboom, Jeroen; Farajzadeh, Rouhi; Rossen, William R.

Important note
To cite this publication, please use the final published version (if applicable).
Please check the document version above.

Injectivity of Multiple Slugs in Surfactant Alternating Gas Foam EOR: A CT Scan Study

J. Gong, Delft University of Technology; **S. Vincent-Bonnieu,** Shell Global Solutions International B.V.;
R. Z. Kamarul Bahrim, C. A. N. B. Che Mamat, R. D. Tewari, and **M. I. Mahamad Amir,** Petronas;
J. Groenenboom, Shell Global Solutions International B.V.; **R. Farajzadeh,** Shell Global Solutions International B.V. and Delft University of Technology; and **W. R. Rossen,** Delft University of Technology

Summary

A surfactant alternating gas (SAG) process is often the injection method for foam, on the basis of its improved injectivity over direct foam injection. In a previous study, we reported coreflood experiments on liquid injectivity after foam flooding and liquid injectivity after injection of a gas slug following steady-state foam. Results showed that a period of gas injection is important for the subsequent liquid injectivity. However, the effects of multiple gas and liquid slugs were not explored.

In this paper, we present a coreflood study of injectivities of multiple gas and liquid slugs in an SAG process in a field core. Nitrogen and surfactant solution are either coinjected or injected separately into the sandstone core sample. The experiments are conducted at an elevated temperature of $90°C$ with a backpressure of 40 bar. Differential pressures are measured to quantify gas and liquid injectivities. Computed tomography (CT) scanning is applied to relate water saturation to mobility.

During the injection of a large gas slug following foam, a bank in which foam completely collapses or greatly weakens forms near the inlet and propagates slowly downstream. During the subsequent period of liquid injection, liquid flows through the collapsed-foam bank much more easily than further downstream. Beyond the collapsed-foam region, liquid first imbibes into the whole cross section. In this region, liquid flows mainly through a finger of high liquid saturation. Our CT results suggest a revision of our earlier interpretation; the process of gas dissolution does not merely follow fingering but is evidently directly involved in the fingering process.

Our results suggest that, in radial flow, the small region of foam collapse very near the well greatly improves injectivity. The subsequent gas and liquid slugs behave near the wellbore, affecting injectivity, in a way similar to the first slugs. Thus, the behavior and modeling of the first gas slug and first subsequent liquid slug is representative of near-well behavior in an SAG process. The trends observed in our previous work are reproduced in a low-permeability field core.

Introduction

Foam, a dispersion of gas in a liquid phase, is widely used in a number of industries, including petroleum production (Harpole et al. 1994; Schramm 1994; Blaker et al. 2002; Skauge et al. 2002; Norris et al. 2014; Mukherjee et al. 2016) and environmental remediation (Wang and Mulligan 2004; Atteia et al. 2013). Foam is applied as an enhanced oil recovery (EOR) technique because of its capability of reducing gas mobility, improving gas-to-liquid mobility ratio, and in turn increasing gas sweep efficiency (Schramm 1994; Rossen 1996; Lake et al. 2014). Foam is also used to recover dense nonaqueous phase liquid in soils in a manner similar to an EOR process (Hirasaki et al. 1997).

Foam can be placed into a reservoir by coinjecting gas and liquid (Rossen et al. 2010) or by a SAG process, where surfactant solution and gas slugs are injected alternatively (Kibodeaux and Rossen 1997; Farajzadeh et al. 2009a, 2009b). SAG is usually the preferred method for foam injection because of its excellent gas injectivity (Matthews 1989; Heller 1994; Shan and Rossen 2004) and its ability to reduce corrosion in pipes and facilities (Matthews 1989; Heller 1994). However, liquid injectivity can be problematic in SAG, and fracturing of the injection well can occur (Kuehne et al. 1990; Martinsen and Vassenden 1999).

Injectivity is, thus, a crucial factor for success of an SAG process. Several studies (Thompson and Gdanski 1993; Kibodeaux et al. 1994; Zeilinger et al. 1995; Morphy et al. 1998; Talabani and Islam 1999; Nguyen et al. 2003; Nguyen et al. 2009) examine liquid injectivity after full-strength foam rather than following a period of gas injection in an SAG process. Most of these studies focus on acid diversion, in which liquid injectivity is extremely poor. This meets the goal of an acid stimulation process. However, this poor liquid injectivity should be avoided in an SAG process. In our previous studies, we examined liquid injectivity directly following foam by conducting coreflood experiments in Berea cores (Gong et al. 2019b). Liquid flows through foam in one or two fingers, leaving the remaining foam trapped in place. The unsaturated liquid dissolves the gas inside and surrounding the liquid fingers. This is consistent with the findings in earlier coreflood studies (Kibodeaux et al. 1994; Nguyen et al. 2009). We also reported in that study gas injectivity after foam and liquid injectivity after injection of a gas slug following steady-state foam. The experimental results indicate that gas-slug injection has massive impacts on the following liquid injectivity. A collapsed-foam region forms near an injection well during the gas injection and slowly propagates further from the well as more gas is injected. This region is crucial to the subsequent liquid injectivity, since liquid mobility in this region during the liquid injection is much greater than that further from the injection well. On the basis of these experimental findings, in a separate paper (Gong et al. 2019a), we proposed a bank-propagation model reflecting the effects of gas injection on the subsequent liquid injectivity. The banks we find in our experiments give a massive improvement in predicted injectivity and are not currently represented in conventional foam simulators.

Multiple gas and liquid slugs are injected in an SAG process. Many studies and field application of an SAG process have been published (Harpole et al. 1994; Grigg et al. 2002; Skauge et al. 2002; Awan et al. 2008; Farajzadeh et al. 2009a, 2009b; Norris et al. 2014; Rossen et al. 2014; Mukherjee et al. 2016). Most of these work were focused on in-situ foam generation, gas injectivity, and gas sweep efficiency in an SAG foam process. Higher gas injectivity compared to coinjection of gas and surfactant solution was observed, as foam

in the near-well region dries out and injectivity increases (Kibodeaux et al. 1997; Shi and Rossen 1998; Shan and Rossen 2002). In a separate study, Rossen and Renkema (2007) conducted a series of simulation of multiple-cycle SAG process with conventional foam simulators. They found that injectivity of later slugs decreases after the first gas- and liquid-slug injection. However, as discussed in our previous work (Gong et al. 2019a, 2019b), there are mechanisms that are not well represented in conventional foam simulators, such as water evaporation into gas, gas dissolution into the liquid fingers, and others. There is a lack of experimental work on the effects of multiple gas and liquid slugs on the injectivity, specifically the effects of the earlier slugs on the injectivity of later slugs. In this paper, we present a series of coreflood experiments of gas and liquid injectivities in a field core. The main goal is to examine the near-well flow behavior during the injection of multiple gas and liquid slugs in an SAG process. We also examine liquid injectivity directly after steady-state foam and following injection of a gas slug after foam, to investigate whether the flow behavior observed in our previous studies also appears in this low-permeability field core.

Materials and Methods

Materials. A nearly homogeneous sandstone field core (Kamarul Bahrim et al. 2017) is used in these experiments. The core has a diameter of 3.8 cm and a length of 6.9 cm. A field core is typically short, though it is possible to butt short cores to make a longer composite core. We do not combine cores for a foam study because of the experimental artifacts included by capillary-end effect at each core boundary (Apaydin and Kovscek 2001). The average porosity of the core is approximately 0.21, and the permeability is approximately 63 md.

A synthetic brine containing five salts [sodium chloride (1.84 wt%), sodium sulfate (0.28 wt%), magnesium chloride (0.73 wt%), calcium chloride (0.1 wt%), and potassium chloride (0.05 wt%)] is used to prepare surfactant solutions. The brine, thus, contains 3 wt% salinity. Surfactant A (Kamarul Bahrim et al. 2017) is used to conduct the foam experiments. The surfactant solution with a concentration of 0.5 wt% is used. Nitrogen with a purity of 99.98% is the gas phase in the foam.

Experimental Setup. The setup used to perform the coreflood experiments is schematically shown in **Fig. 1.** The core is coated with epoxy and built into a polyether ether ketone core holder, which is appropriate for CT scanning because of its low X-ray attenuation. The core holder is fixed horizontally and coated with a thermal jacket, with heated silicon oil flowing through it, to hold the temperature of the core at approximately 90°C. Two absolute-pressure transducers and two differential-pressure transducers are used to monitor the absolute pressures at various positions along the core, as well as the pressure drops across the entire core (ΔP_t) and across the middle section of the core (Section 2, ΔP_2). In this work, we study the middle section (Section 2), which has a length of 4.2 cm, to avoid the entrance region (Ransohoff and Radke 1988) and the capillary-end effects (Apaydin and Kovscek 2001). A Quizix pump is used to inject surfactant solution and control the liquid injection rate. Nitrogen is provided from a gas cylinder and injected into the core through a mass flow controller. A backpressure regulator is applied to maintain the backpressure at 40 bar.
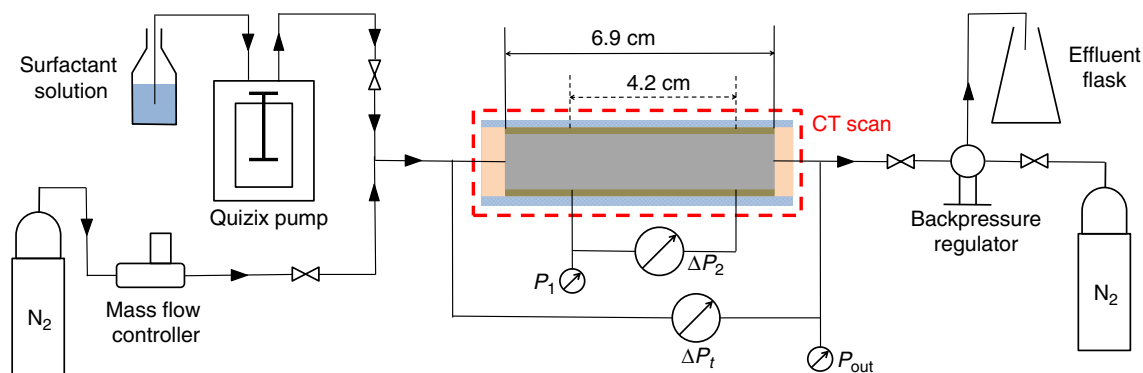

Fig. 1—Schematic representation of the experimental setup.

A third-generation Siemens SOMATOM CT scanner is used to visualize water-saturation changes and relate the change in water saturation to that in pressure difference measured in the experiments. The CT scanner is operated with single energy at a voltage of 140 keV and a current of 250 mA. To obtain the water-saturation profiles both at cross sections and along the core, we scan the entire core each time. The thickness of each cross-sectional CT slice is 6 mm. The resolution of each cross section is 521×521 pixels. An imaging software package ImageJ (Schindelin et al. 2012) is applied to visualize the three-dimensional (3D) CT images and perform the image analysis.

Experimental Method. In all experiments, we first inject 0.95-quality (gas fractional flow) foam into the core by coinjecting gas (nitrogen) and surfactant solution. The total superficial velocity for foam injection is 1 ft/d. The quality 0.95 is chosen for comparison with our previous work with Berea cores (Gong et al. 2019b). In the subsequent gas- and liquid-injection periods, gas and surfactant solution are injected at superficial velocities of 6 and 1 ft/D, respectively.

In this study, we present three experiments (Cases A–C) to examine gas and liquid injectivities under various conditions. We first study the liquid injection directly following 0.95-quality foam (Case A). We then examine a prolonged period of gas injection after foam, and a following liquid-injection period (Case B). Finally, the injection of multiple large gas and liquid slugs is studied (Case C). In this case, we inject multiple gas and liquid slugs in the following sequence: foam—first gas slug—first liquid slug—second gas slug—second liquid slug. In all experiments, there is no oil in the system. In a field application, oil may well have been displaced from the near-well region before or soon after the start of the SAG process.

Experiments and Results

Because the experiments are conducted in a short field core, it is important to know whether the section studied avoids the entrance and capillary-end effects. As shown in **Fig. 2,** in the region of interest, the average cross-sectional water saturations during the initial steady-state foam injection in Cases A–C are roughly uniform at 0.32 (Fig. 2). This suggests that the region studied is relatively free of entrance and capillary-end effects.
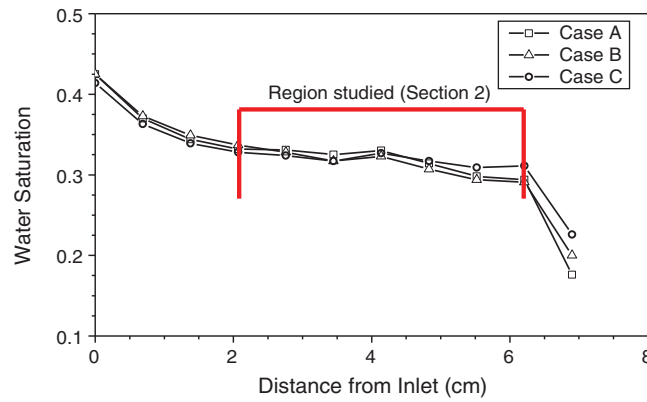
Fig. 2—Water-saturation profile in initial steady-state foam (0.95-quality) in Cases A–C.

Case A: Liquid Injection Follows Foam. In this experiment, we inject surfactant solution directly after full-strength foam. As shown in **Fig. 3,** the pressure gradient evolves over three stages. In the beginning, liquid flows into the core with a relatively high mobility (the initial low pressure gradient). The pressure gradient then reaches a large value and holds constant for a period of approximately 2.5 pore volumes (PV). During this period, liquid imbibes throughout the core cross section (Fig. 3b). After approximately 3.5 PV of liquid is injected, a finger with much greater water saturation is visible at this position 3 cm from the inlet (Fig. 3c). The pressure gradient then decreases, as the liquid finger advances across the given core section.
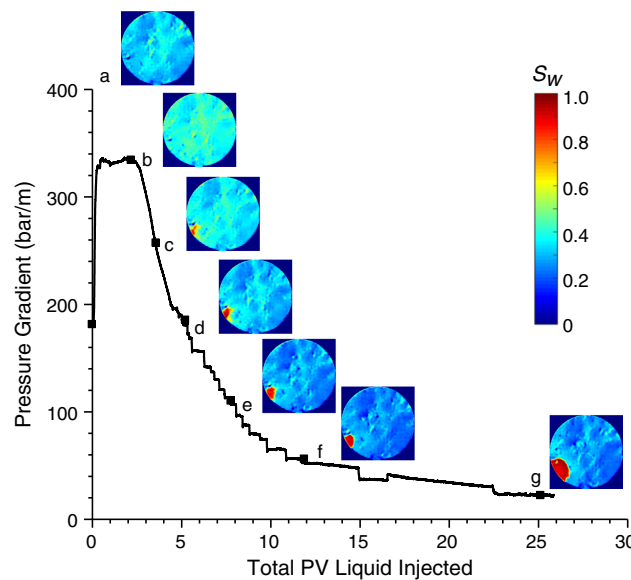

Fig. 3—Pressure gradient in Section 2 during the liquid injection directly after steady-state foam ($f_g = 0.95$): (a–g) water saturation at a position 3 cm from the inlet after different periods of liquid injection—(a) initial state (steady-state foam), (b) 2.7 PV, (c) 3.5 PV, (d) 5.6 PV, (e) 7.8 PV, (f) 11.8 PV, and (g) 25.3 PV.

As shown in Figs. 3a and 3b, at this position 3 cm from the inlet, the entire cross section turns from light blue to light green, indicating that the water saturation of the whole cross section increases. A liquid finger is then observed after approximately 3.5 PV of liquid is injected (Fig. 3c) with substantially greater water saturation. The liquid finger progresses forward and widens as more liquid is injected (Figs. 3d through 3g). Over time, the liquid finger also becomes more red, which confirms that the unsaturated liquid dissolves or displaces additional gas trapped inside the liquid finger. In the meantime, the region outside the liquid finger turns to a deeper blue, which indicates that gas outside the finger remains trapped in place. Gas expands as absolute pressure declines and drives down water saturation further in this region.

In our earlier study (Gong et al. 2019b), we referred to a fingering process followed by gas dissolution into the finger. An analysis of the CT images in **Figs. 3 and 4** supports a revised interpretation, indicating that the process of gas dissolution is important in the fingering process.

In Fig. 4c, we analyze a region that lies within the finger from its first appearance (Fig. 4a; compare with Fig. 3c) and a region that remains outside the finger throughout the images (Fig. 4b; compare with Fig. 3g). The average water saturation both inside and outside the liquid finger increases from 0.3 (steady-state foam) quickly to approximately 0.4 and remains nearly constant until approximately 2.7 PV of liquid injection (Fig. 4c). This suggests that ahead of the liquid finger, liquid flow disperses across the core cross section without fingering (see also Fig. 3b). Thereafter, a finger, with distinctly greater water saturation, appears. Water saturation inside the finger increases and finally reaches approximately 0.9, indicating that gas trapped within the liquid finger has dissolved into liquid or been displaced. In our previous study (Gong et al. 2019b), we showed that the rise in liquid saturation within the finger and the progress of the finger through the core roughly correspond to the rate of gas dissolution expected for N_2 under our experimental conditions. This dissolution causes a huge rise in water relative permeability within the finger and subsequent diversion of virtually all water through the

finger. As proposed by O'Sullivan and Smith (1970), 1 PV of brine can dissolve approximately 0.012 PV of N_2 at 90°C. As shown in Fig. 4, liquid flows through approximately 1/15 of the core cross section. A measure of 3 PV of liquid would dissolve enough N_2 to change the water saturation within the liquid finger by $(0.012 \times 3 \times 15) \approx 54\%$, which is in agreement with the change in water saturation shown in Fig. 4. This sequence suggests that gas dissolution plays a key role in the formation of the finger, raising water relative permeability and directing liquid to flow within the finger along its length. Even ahead of the finger, water flows into the trapped foam primarily from the tip of the finger. This process is analogous to wormhole formation in acidization of carbonates, where greater flow of acid leads to greater dissolution and, in turn, yet-greater flow of acid through the wormhole (Hoefner et al. 1987). Once the finger is evident, water saturation outside the liquid finger decreases to approximately 0.1 as more surfactant solution is injected (Fig. 4c). Gas outside the liquid finger remains trapped.
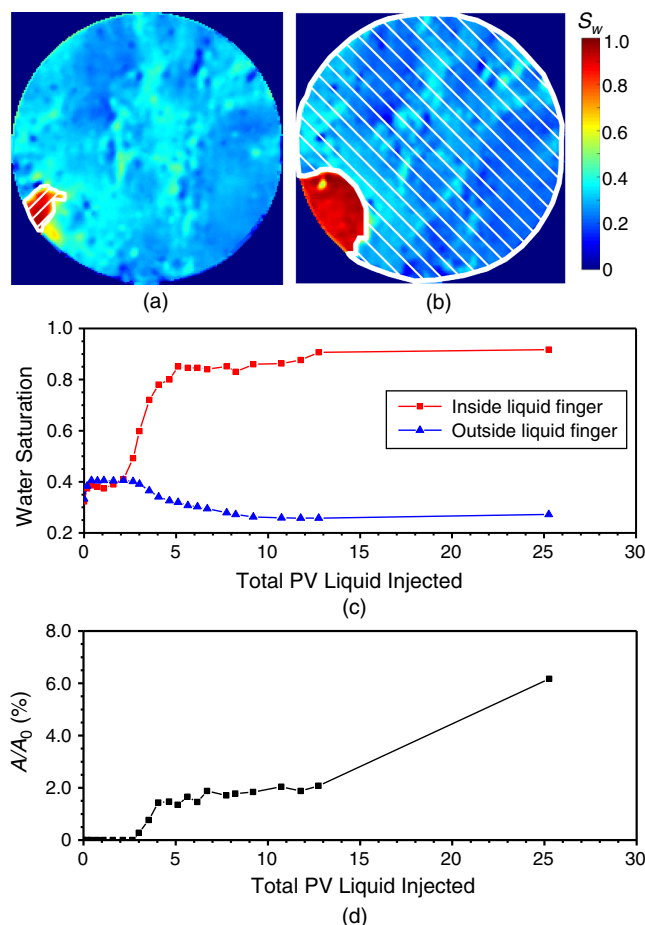
Fig. 4—Liquid finger at a position 3 cm from the inlet: (a) region that lies inside the liquid finger (the shaded area) from its first appearance, (b) region that lies outside the liquid finger (the shaded area) in all images, (c) average water saturation inside and outside the liquid finger, and (d) dimensionless area of the liquid finger as a function of time. *A* is the area of the liquid finger (i.e., with S_w larger than 0.65); A_0 is the area of the entire cross section.

In Fig. 4d, we estimate the area with distinctly higher water saturation in the cross-sectional images. As shown in Fig. 4d (compare with Figs. 3a and 3b), there is no region of distinctly greater water saturation evident in the CT-saturation image until approximately 2.7 PV of liquid injection. The finger becomes evident as dissolution of gas within the finger greatly changes gas saturation there. The liquid finger is first evident in the CT image, occupying approximately 1.5% of the cross section, after approximately 4 PV of liquid injection (compare with Fig. 3c). The finger size remains nearly unchanged for about 10 PV of liquid injection (from 4 to 14 PV) and then grows slowly outward as it dissolves surrounding trapped gas (compare with Figs. 3d through 3g).

Gas solubility, thus, plays an important role during the liquid injection in an SAG process. More-soluble gas, such as CO_2, would lead to faster gas dissolution into water and faster propagation of the gas-dissolution front during the liquid injection. Liquid evaporation and foam collapse during the gas injection could also be different under different conditions, along with foam mobility.

Case B: Injection of Single Gas and Liquid Slugs. In this experiment, we inject surfactant solution following a prolonged period of gas injection (approximately 640 PV) that, in turn, follows steady-state foam injection (0.95 quality). During the gas-injection period, the pressure gradient in Section 2 first decreases from 250 bar/m to a plateau value (approximately 50 bar/m), which lasts for approximately 220 PV of gas injection (from approximately 40 PV to approximately 260 PV), and then experiences a second decline **(Fig. 5a)**. The pressure gradient remains substantial in Section 2 until a sufficient amount of gas is injected, i.e., approximately 470 PV. The subsequent decline in pressure gradient implies that foam greatly weakens or collapses after sufficient gas injection. This could reflect a continuous-gas foam with some gas still trapped in place (Rossen 1996).

This is confirmed by CT scans (Figs. 5b and 5c). As shown in Fig. 5b, the initial water saturation when the core is saturated with 0.95-quality foam is approximately 0.35 (the light green color in Fig. 5c). After approximately 34.1 PV of gas injection, the average cross section water saturation decreases to approximately 0.25 along the whole core (the light blue color in Fig. 5c), which indicates

that gas first flushes the whole core, which makes foam in the entire core weaker. Water saturation then decreases in a wave moving downstream, i.e., from the positions 1.8–5.4 cm from the inlet (Fig. 5b), which indicates that a region of collapsed or greatly weakened foam propagates slowly from the inlet downstream. The propagation of the collapsed-foam region can be seen in Fig. 5c: a dark blue region (marked by a yellow arrow) propagates toward the outlet (right side) as more gas is injected. After approximately 640 PV of gas is injected, the collapsed-foam bank reaches the end of the core.
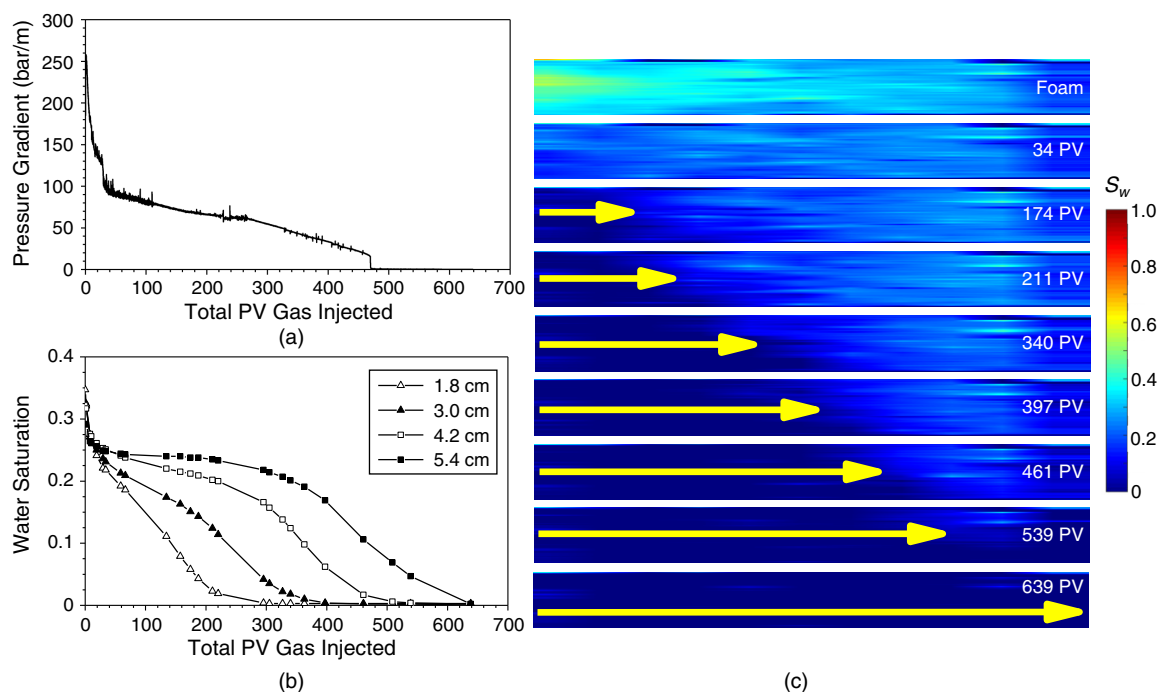
Fig. 5—Pressure gradient and water saturation during a prolonged period of gas injection following steady-state foam ($f_g = 0.95$): (a) pressure gradient in Section 2 during the gas injection following 0.95-quality foam; (b) average water saturation during the gas injection in cross sections at four different positions: 1.8, 3, 4.2, and 5.4 cm from the inlet; and (c) water-saturation profile in a vertical cross section along the central axis of the core. The yellow arrows show the propagation of the collapsed-foam region.

Thus, during a gas-injection period, gas first weakens foam. Foam then collapses or greatly weakens when an adequate volume of gas is injected. The collapsed-foam region moves as a wave from the inlet downstream as more gas is injected. The interplay of water evaporation, pressure-gradient-driven flow, and capillary effects leads to foam weakening and collapse (Gong et al. 2019b).

This result is similar to that in our previous study (Gong et al. 2019a), in that prolonged gas injection leads to a collapsed-foam region that slowly propagates from the core face downstream. However, the collapsed-foam region advances more slowly and with a larger total mobility ($1/588$, 9.9×10^{-10} m^2/Pa·s) in this field core than in the Berea cores ($1/400$, 9×10^{-10} m^2/Pa·s). In the coreflood experiments with Berea cores, foam collapsed at a water saturation of approximately 0.2. In this case, the water saturation at the point of foam collapse is approximately 0.1, as measured in the CT images. That is, the rise in mobility occurs when water saturation falls to approximately 0.1; water saturation then continues to fall further. We believe that the water saturation after prolonged gas injection is very small but not zero. The calculation on the basis of CT measurements can be affected by the noise in images. For purpose of injectivity, the key event is the collapse of foam at a water saturation of approximately 0.1.

Thus, a collapsed-foam bank is created after a sufficient amount of gas was injected and slowly propagates from the inlet of the core. This is expected to have a massive impact on the following liquid-injection period. In our experiments, after approximately 640 PV of gas is injected, foam in the entire core collapses or weakens greatly, making the subsequent liquid injection 23 times easier (pressure gradient 23 times lower) than in liquid injection directly following foam (Case A). However, the pressure gradient is still 15 bar/m (not shown), which suggests that some gas remains trapped. This is confirmed by CT measurements during the subsequent liquid injection (**Fig. 6**).

Fig. 6a shows the vertical axial water-saturation profile during the liquid injection after 640 PV of gas is injected, when the collapsed-foam bank occupies the whole core (Fig. 5c). Liquid initially imbibes into the entire cross section without fingering (0.27–0.97 PV of liquid injection in Fig. 6a). This suggests that foam collapses or greatly weakens after a sufficient amount of gas injection, leaving some trapped gas, and, in turn, makes the subsequent liquid injection much easier than following full-strength foam. After a longer period of liquid injection (8.6 PV), a high-water-saturation region appears near the bottom of the core starting at the inlet (the red region). This suggests that preferential paths for liquid flow develop within the collapsed-foam region; these can be seen more clearly in Fig. 6b. Since the mobility within this region is already high compared to intact foam further from the well, this would be expected to make only a minor difference to overall injectivity (Gong et al. 2019a).

Fig. 6b presents the water-saturation profile at a position 3 cm from the inlet over time. The cross section is dark blue after approximately 0.27 PV of liquid injection, since liquid has not yet arrived at this position. After approximately 1.9 PV of liquid is injected, the whole cross section has turned to light yellow, reflecting liquid sweep of the entire cross section. Starting from 5.8 PV of liquid injection, some regions turn red as more liquid is injected. This confirms that liquid finds preferential paths after approximately 5.8 PV of liquid injection. The liquid preferential paths expand outward over time.

Case C: Injection of Multiple Gas and Liquid Slugs. In this experiment, we examine the injectivity of multiple (more than one each) gas and liquid slugs. The gas and liquid slugs are injected in the following sequence: 0.95-quality foam injection; first gas slug

(approximately 250 PV); first liquid slug (approximately 26 PV); second gas slug (approximately 150 PV); second liquid slug (approximately 38 PV). The pressure gradients and the water-saturation profiles during the injection of the two gas slugs and the two liquid slugs are compared, respectively.
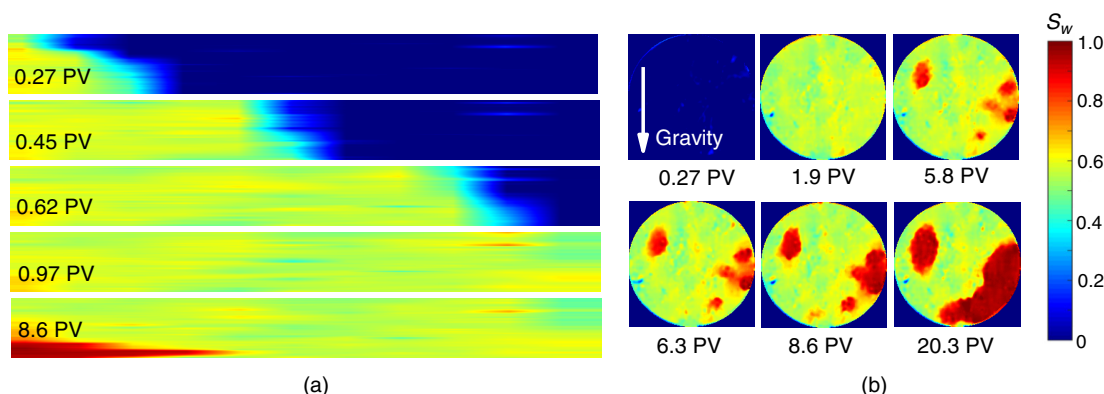
Fig. 6—Water-saturation profile during liquid-injection period following a period of gas injection (approximately 640 PV) after steady-state foam ($f_g = 0.95$): (a) water-saturation profile in a vertical cross section along the central axis of the core and (b) water-saturation profile at a cross section 3 cm from the inlet after different amounts of liquid injection.

As shown in **Fig. 7,** overall, the two gas slugs show a similar behavior in pressure gradient. The pressure gradients for both the first and the second gas slugs quickly reach a peak and then decrease to a plateau. The peak values of pressure gradient for the two gas slugs are comparable, approximately 220 bar/m for the first gas slug and approximately 250 bar/m for the second gas slug, which indicates that the two gas slugs quickly reach a similar state.
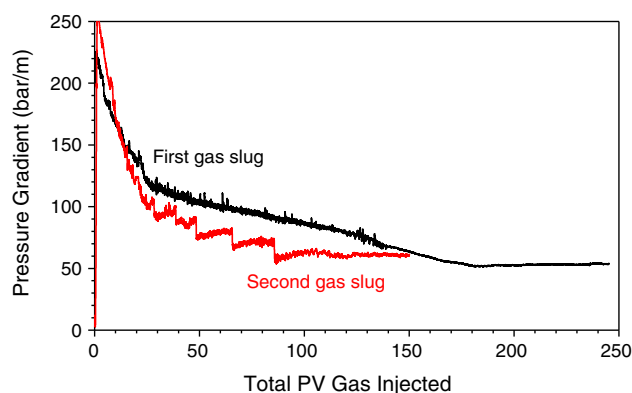
Fig. 7—Pressure gradient in Section 2 during the first and second gas slug injection in an SAG process.

As mentioned above, the core is saturated with steady-state foam before injection of the first gas slug, while a period of liquid injection (the first liquid slug) precedes the second gas slug. Thus, the similarity in the peak values of the pressure gradients implies that strong foam is generated in the beginning of the injection of the second gas slug. An SAG process works well in generating foam in this case. This is confirmed by the CT measurements.

Fig. 8 shows the average cross-sectional water saturation at four locations along the core, during the injection of the first (Fig. 8a) and the second (Fig. 8b) gas slugs. During the injection of the first gas slug, the initial water saturation is approximately 0.3 for all four positions (reflecting steady-state foam). During the injection of the second gas slug, water saturation starts from values greater than 0.3, because a liquid slug was injected beforehand. For the position 1.8 cm from the inlet, the initial water saturation is approximately 0.65. The main reason is that the position 1.8 cm from the inlet is within the collapsed-foam region created during the first period of gas injection; the first liquid slug then sweeps the entire cross section with a high water saturation. The water saturation then quickly decreases to approximately 0.3 for all the positions, as gas displaces liquid in the core and foam is generated. Thereafter, the water saturation for the two gas slugs follows nearly the same trend. At the position 1.8 cm from the inlet, the average cross-sectional water saturation decreases gradually to approximately 0.1 after approximately 150 PV of gas is injected (Figs. 8a and 8b) and to nearly zero after approximately 250 PV of gas is injected (Fig. 8a). However, at a position further downstream, close to the outlet, i.e., 5.4 cm from the inlet, the water saturation holds nearly constant during this period. This means that foam collapses at the position 1.8 cm from the inlet, while 5.4 cm from the inlet is beyond the collapsed-foam region (Figs. 8a and 8b).

Fig. 9 shows the axial water-saturation profile during the injection of the two gas slugs. A wide liquid finger forms near the inlet during the injection of the first liquid slug (compare with Fig. 9b, top; compare with Fig. 6). The liquid finger disappears quickly as gas flows in (Fig. 9b, subsequent CT images). After approximately 1.2 PV of gas injection in the second gas slug, the water-saturation profile becomes similar to the initial state during the injection of the first gas slug (steady-state foam). This confirms that foam is generated quickly as the second gas slug is injected. As more gas is injected, the collapsed-foam region propagates downstream from the inlet. The front of the collapsed-foam region arrives at a similar position after a similar amount of gas is injected, i.e., 141 PV for the first gas slug and 150 PV for the second gas slug (images in the bottom row of Figs. 9a and 9b). This suggests that the collapsed-foam region propagates with similar velocities during the two periods of gas injection.
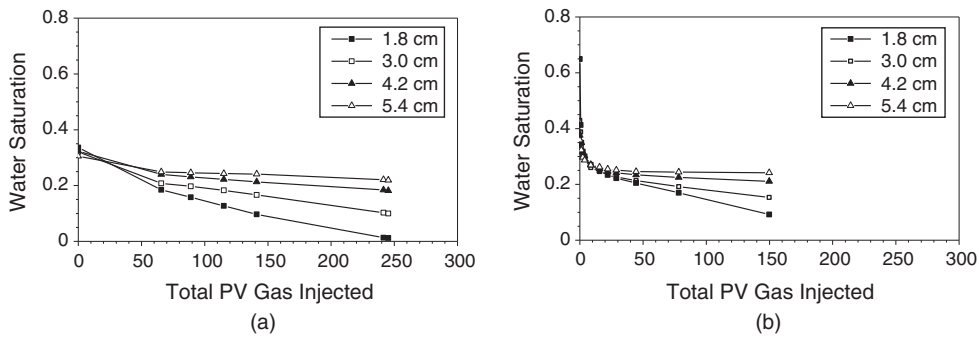
Fig. 8—Average water saturation in the entire cross section at different positions along the core during the gas injection: (a) first gas slug injection and (b) second gas slug injection.
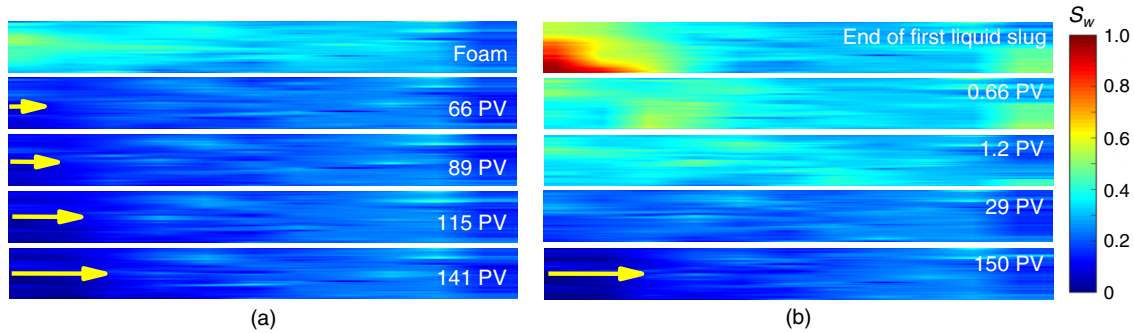

Fig. 9—Water-saturation profile in a vertical cross section along the central axis of the core during the gas-injection periods: (a) first gas slug and (b) second gas slug.

Thus, the second gas slug behaves like the first gas slug, both within and beyond the collapsed-foam region.

During the first and the second periods of liquid injection, the pressure gradient first rises to a large value, remains nearly constant for a time, and then decreases to a small value **(Fig. 10).** The pressure gradient in both cases has a similar shape to that for liquid injection directly following foam (Case A). However, the plateau values of the pressure gradient for the first and the second periods of liquid injection in an SAG process are smaller than the value for the case where liquid is injected directly after foam, which is approximately 340 bar/m (compare with Fig. 3). The plateau pressure gradient during the injection of the first liquid slug is smaller than that during the injection of the second liquid slug. The reason is that a larger gas slug was injected before the first liquid slug (250 PV) than before the second liquid slug (150 PV). The larger gas slug creates a larger collapsed-foam region in the core, which, in turn, reduces the pressure gradient during the subsequent liquid injection. This is supported by the CT measurements. As shown in **Fig. 11,** at the end of the injection of the first and second gas slugs, there are dark blue regions on the left side of the images for both gas slugs. The dark blue region is larger at the end of the injection of the first gas slug than at the end of the injection of the second gas slug; the collapsed-foam region is larger before the injection of the first liquid slug.
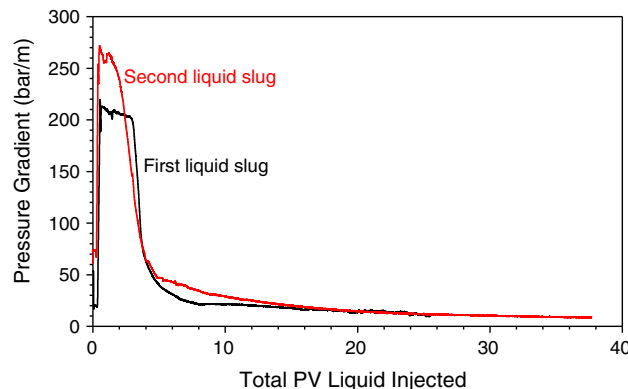

Fig. 10—Pressure gradient in Section 2 during the injection of the first and second liquid slugs in an SAG process.

When liquid is injected, the two liquid slugs behave similarly: liquid first rapidly occupies the collapsed-foam region (the yellow region on the left side of the images on the second row in Fig. 11), in which there is less trapped gas. As more liquid is injected, the water saturation in the middle of the core becomes more red over time in the collapsed-foam region, while beyond the collapsed-foam region, it first turns to light green and then to light blue (Fig. 11). However, what happens in the weakened-foam region cannot be fully seen from the axial CT images, since the liquid flow path can be tortuous, moving in and out of this axial cross section. In order to understand the flow behavior in the weakened-foam region during the two liquid-injection periods, we study the cross-sectional water-saturation profiles perpendicular to the axis of the core **(Figs. 12 and 13).**
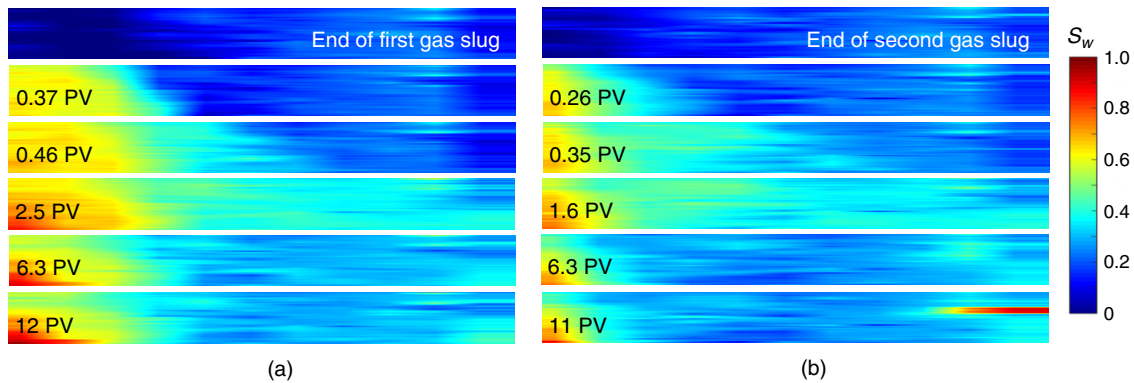
Fig. 11—Water-saturation profile in a vertical cross section along the central axis of the core during the liquid injection: (a) first liquid slug and (b) second liquid slug.
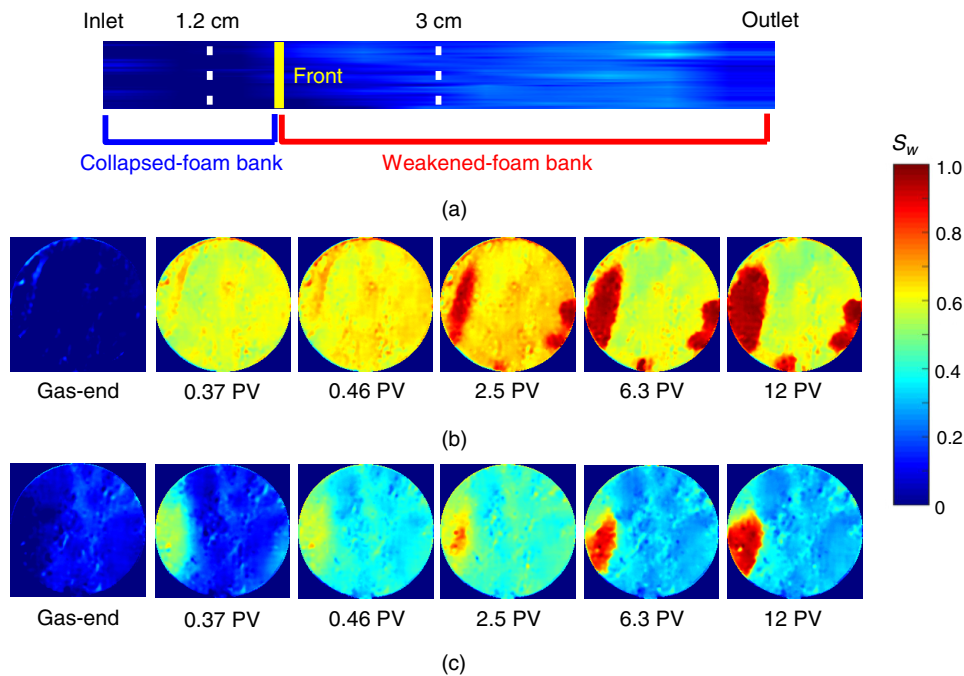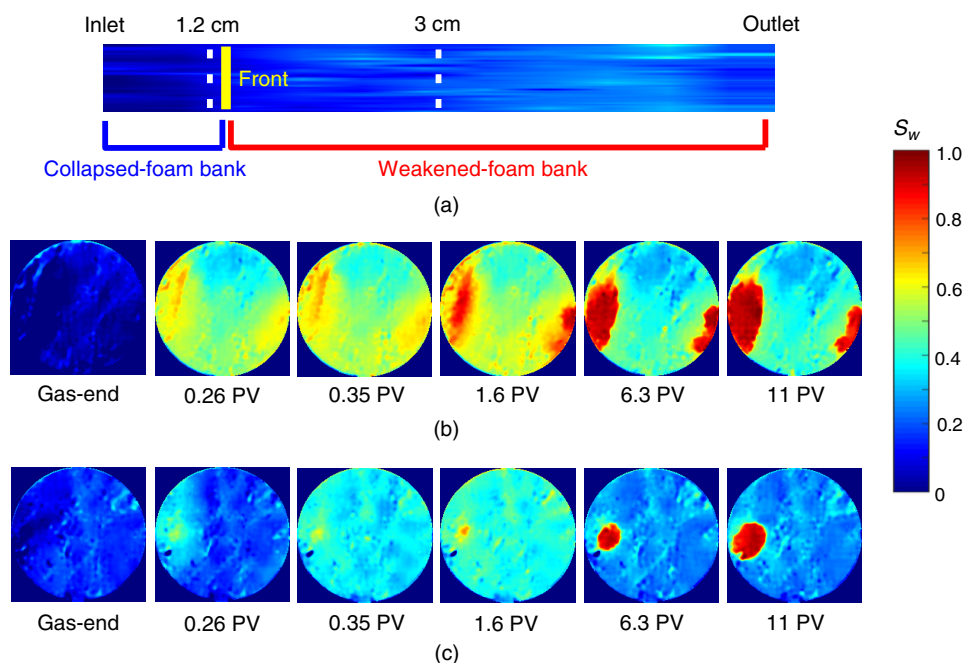

Fig. 12—Water-saturation profile during the first liquid slug injection: (a) axial vertical cross section showing collapsed-foam bank and weakened-foam bank created before injection of the first liquid slug, (b) water-saturation profile at a position within the collapsed-foam bank (1.2 cm from the inlet) after different amounts of liquid injection, (c) water-saturation profile at a position beyond the collapsed-foam bank (3 cm from the inlet) after different amounts of liquid injection.

Fig. 12 shows the average water saturation in cross sections during the injection of the first liquid slug. As presented in Fig. 12a, at the end of the injection of the first gas slug, the core is occupied by two banks, the collapsed-foam bank and the weakened-foam bank. The yellow line represents the front of the collapsed-foam bank. The water saturations over time at two positions are presented, one within the collapsed-foam region (1.2 cm from the inlet, Fig. 12b) and the other beyond the collapsed-foam region (3 cm from the inlet, Fig. 12c). In the collapsed-foam region, liquid first flushes the entire cross section and then forms preferential paths after a period of liquid injection, i.e., 2.5 PV in this case (Fig. 12b). In the weakened-foam region, liquid does not sweep the entire cross section. Liquid penetrates foam through a finger as in the case where liquid is injected right after full-strength foam (Fig. 12c). The liquid finger is observable after approximately 2.5 PV of surfactant solution is injected. In the second cross section (Fig. 12c), the link between gas dissolution and fingering is less immediate than that in Fig. 3. The preferential flow path along the left side proceeds from blue to yellow to red and then widens gradually over time. Ahead of the collapsed-foam region, the formation of the fingers depends in part on preferential flow paths developing within the collapsed-foam bank (Fig. 12b).

Fig. 13 presents water saturation at the same two positions along the core during the injection of the second liquid slug. Similar to the first liquid slug, liquid first rapidly flows through the collapsed-foam region with high mobility and then the fingers through trapped gas beyond the collapsed-foam region in a pattern reflecting preferential flow paths developing in the collapsed-foam bank.

In general, foam in this relatively low-permeability field core behaves similar to its behavior in the Berea cores (Gong et al. 2019b) during the injection of a liquid slug after a gas-slug injection following foam. Liquid first fills the collapsed-foam bank quickly and then penetrates the weakened-foam bank through the liquid fingers. Gas within and surrounding the liquid fingers dissolves or is displaced over time. However, compared with the results with the Berea cores (Gong et al. 2019a), in this case, the liquid-fingering bank propagates more slowly with a lower total mobility (1.4, 1.4×10^{-13} m²/Pa·s). The gas-dissolution bank propagates with a greater dimensionless velocity and a lower total mobility (0.2, 2×10^{-12} m²/Pa·s). The corresponding values for the Berea cores were 3.3 (dimensionless velocity) and 8.5×10^{-13} m²/Pa·s (total mobility) for the liquid-fingering bank and 0.08 (dimensionless velocity) and 6.6×10^{-11} m²/Pa·s (total mobility) for the gas-dissolution bank (Gong et al. 2019a).

Fig. 13—Water-saturation profile during the injection of the second liquid slug: (a) collapsed-foam bank and weakened-foam bank created before injection of the first liquid slug, (b) water-saturation profile at a position within the collapsed-foam bank (1.2 cm from the inlet) after different amounts of liquid injection, and (c) water-saturation profile at a position beyond the collapsed-foam bank (3 cm from the inlet) after different amounts of liquid injection.

Fig. 14 compares the properties of the liquid finger at the same position (3 cm from the inlet, beyond the collapsed-foam region) during the two periods of liquid injection. In general, the second liquid slug behaves like the first liquid slug. The initial water saturation outside the liquid finger is also approximately 0.2. Similar to what we observed in liquid injection directly following foam (Case A), the average water saturation outside the liquid finger first quickly reaches a plateau at approximately 0.45, which lasts approximately 2.5 PV, and then decreases to approximately 0.25–0.3 over time (Fig. 14a). Unlike liquid injection directly following foam (Case A), the average water saturation inside the liquid finger increases from approximately 0.2 (after a period of gas injection) to approximately 0.9 within a short time. In contrast, water saturation outside the finger holds steady (compare with Fig. 4). One possible reason is that a gas-slug injection weakens foam, making it easier for liquid to form a finger. Another possible reason is that formation of preferential flow paths in the collapsed-foam region promotes fingering in the foam bank beyond it. Figs. 12 and 13 show that the liquid fingers become visible more quickly (within 1 PV of liquid injection) than with liquid injection directly following foam. The liquid finger grows outward as more liquid is injected for both liquid slugs, although the liquid finger formed during the injection of the second liquid slug is smaller than that formed during the injection of the first liquid slug (Fig. 14b).
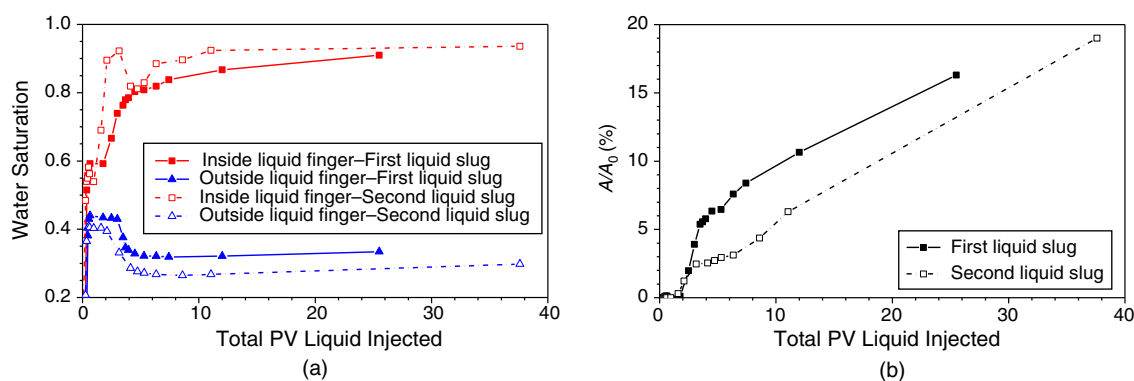
Fig. 14—Liquid finger visible at 3 cm from the inlet: (a) water saturation inside and outside the liquid finger during the injection of the first and second liquid slugs and (b) dimensionless area of the liquid finger during the injection of the first and second liquid slugs. A is the area of the liquid finger (S_w larger than 0.65); A_0 is the total area of the cross section.

Conclusions

In this work, we present the first coreflood study of the near-well effects during injection of multiple gas and liquid slugs in an SAG-foam process. We observe the following behavior.
- Liquid injectivity directly after full-strength foam is extremely poor, as reported previously in the literature.
- Gas dissolution can play a key role in the formation of the liquid finger, directing liquid to flow through the finger and to increasing liquid injectivity.

- In an SAG process, during the injection of a large gas slug after foam, gas first weakens foam in the entire core. Then, a collapsed-foam region begins near the inlet and propagates slowly downstream. This collapsed-foam region has major impact on subsequent liquid injectivity.
- During the subsequent liquid injection, liquid sweeps the entire core cross section in the collapsed-foam region, while the liquid fingers through the weakened-foam region.
- An SAG process forms strong foam quickly when gas flows in, despite the presence of the liquid finger at the end of previous liquid-slug injection.
- The behavior of the first gas and liquid slugs is representative of gas and liquid injectivities of later slugs in an SAG process.

With different gas, formation, temperature, salinity, or surfactant, detailed behavior would be different. The mobility in the banks, bank-propagation velocities, gas solubilities, and liquid evaporation rates would also be different, along with foam mobility. Liquid evaporation plays a role in the collapsed-foam bank and gas solubility in fingering/gas-dissolution bank (Gong et al. 2019a, 2019b). But we expect that the overall trends would be similar in other cases.

The pressure gradient discussed here is larger than often expected in the field. The permeability of the reservoir core used in this study is relatively low, approximately 63 md, which is one of the reasons for the high pressure gradient. We also did similar experiments (Gong et al. 2019a) with Berea cores (approximately 150 md permeability) and Bentheimer cores (approximately 2 darcies permeability). For the Bentheimer cores, in the worst case of liquid injectivity (liquid injection following full-strength foam), the highest pressure gradient is approximately 20 bar/m. The behavior observed was similar at lower pressure gradient.

In our previous work (Gong et al. 2019a), we proposed a simple bank-propagation model based directly on the coreflood experiments and showed the implications of the behavior like that seen in this study for injectivity in SAG processes. This work shows that the model could be applied to the near-well region in an SAG process with multiple slugs. Current foam models do not represent fine-scale liquid fingering, capillary trapping of gas in foam, gas dissolution, and water evaporation well. These effects have major impacts on liquid injectivity in an SAG process.

Nomenclature

A = area of the liquid finger, m^2
A_0 = area of the entire cross section, m^2
f_g = gas fractional flow, dimensionless
PV = pore volumes, dimensionless
S_w = water saturation, dimensionless
ΔP_t = pressure drop across the entire core, bar
ΔP_2 = pressure drop across the middle section of the core, bar

Acknowledgments

References

Apaydin, O. G. and Kovscek, A. R. 2001. Surfactant Concentration and End Effects on Foam Flow in Porous Media. *Transp Porous Media* **43** (3): 511–536. https://doi.org/10.1023/A:1010740811277.

Atteia, O., Estrada, E. D. C., and Bertin, H. 2013. Soil Flushing: A Review of the Origin of Efficiency Variability. *Rev Environ Sci Bio/Technol* **12** (4): 379–389. https://sci-hub.tw/10.1007/s11157-013-9316-0.

Awan, A. R., Teigland, R., and Kleppe, J. 2008. A Survey of North Sea Enhanced-Oil-Recovery Projects Initiated during the Years 1975 to 2005. *SPE Res Eval & Eng* **11** (3): 497–512. SPE-99546-PA. https://doi.org/10.2118/99546-PA.

Behenna, F. R. 1995. Acid Diversion from an Undamaged to a Damaged Core Using Multiple Foam Slugs. Paper presented at the SPE European Formation Damage Conference, The Hague, The Netherlands, 15–16 May. SPE-30121-MS. https://doi.org/10.2118/30121-MS.

Blaker, T., Aarra, M. G., and Skauge, A. 2002. Foam for Gas Mobility Control in the Snorre Field: The FAWAG Project. *SPE Res Eval & Eng* **5** (4): 317–323. SPE-78824-PA. https://doi.org/10.2118/78824-PA.

Farajzadeh, R., Andrianov, A., Bruining, H. et al. 2009a. Comparative Study of CO_2 and N_2 Foams in Porous Media at Low and High Pressure-Temperatures. *Ind Eng Chem Res* **48** (9): 4542-4552.

Farajzadeh, R., Andrianov, A., and Zitha, P. L. J. 2009b. Investigation of Immiscible and Miscible Foam for Enhancing Oil Recovery. *Ind Eng Chem Res* **49** (4): 1910–1919. https://doi.org/10.1021/ie901109d.

Gong, J., Vincent Bonnieu, S., Kamarul Bahrim, R. Z. et al. 2019a. Modelling of Liquid Injectivity in Surfactant-Alternating-Gas Foam Enhanced Oil Recovery. *SPE J.* **24** (3): 1123–1138. SPE-190435-PA. https://doi.org/10.2118/190435-PA.

Gong, J., Vincent Bonnieu, S., Kamarul Bahrim, R. Z. et al. 2019b. Laboratory Investigation of Liquid Injectivity in Surfactant-Alternating-Gas Foam Enhanced Oil Recovery. *Transp Porous Media*: 1–15. https://doi.org/10.1007/s11242-018-01231-5.

Grigg, B. R., Tsau, J. S., and Martin, F. D. 2002. Cost Reduction and Injectivity Improvement for CO_2 Foams for Mobility Control. Paper presented at the SPE/DOE Improved Oil Recovery Symposium, Tulsa, Oklahoma, USA, 13–17 April. SPE-75178-MS. https://doi.org/10.2118/75178-MS.

Harpole, K. J., Siemers, W. T., and Gerard, M. G. 1994. CO_2 Foam Field Verification Pilot Test at EVGSAU: Phase IIIC—Reservoir Characterization and Response to Foam Injection. Paper presented at the SPE/DOE Improved Oil Recovery Symposium, Tulsa, Oklahoma, USA, 17–20 April. SPE-27798-MS. https://doi.org/10.2118/27798-MS.

Heller, J. P. 1994. CO_2 Foams in Enhanced Oil Recovery. In *Foams: Fundamentals and Applications in the Petroleum Industry*, ed. L. L. Schramm, Vol. 242, Chapter 5, 201–234. Washington, DC, USA: American Chemical Society. https://doi.org/10.1021/ba-1994-0242.ch005.

Hirasaki, G., Miller, C. A., Szafranski, R. et al. 1997. Field Demonstration of the Surfactant/Foam Process for Aquifer Remediation. Paper presented at the SPE Annual Technical Conference and Exhibition, San Antonio, Texas, USA, 5–8 October. SPE-39292-MS. https://doi.org/10.2118/39292-MS.

Hoefner, M. L., Fogler, H. S., Stenius, P. et al. 1987. Role of Acid Diffusion in Matrix Acidizing of Carbonates. *J Pet Technol* **39** (2): 203–208. SPE-13564-PA. https://doi.org/10.2118/13564-PA.

Kamarul Bahrim, R. Z., Zeng, Y., Vincen Bonnieu, S. et al. 2017. A Study of Methane Foam in Reservoir Rocks for Mobility Control at High Temperature with Varied Permeabilities: Experiment and Simulation. Paper presented at the SPE/IATMI Asia Pacific Oil and Gas Conference and Exhibition, Jakarta, Indonesia, 17–19 October. SPE-186967-MS. https://doi.org/10.2118/186967-MS.

Kibodeaux, K. R., and Rossen, W. R. 1997. Coreflood Study of Surfactant-Alternating-Gas Foam Processes: Implications for Field Design. Paper presented at the SPE Western Regional Meeting, Long Beach, California, USA, 25–27 June. SPE-38318-MS. https://doi.org/10.2118/38318-MS.

Kibodeaux, K. R., Zeilinger, S. C., and Rossen, W. R. 1994. Sensitivity Study of Foam Diversion Processes for Matrix Acidization. Paper presented at the SPE Annual Technical Conference and Exhibition, New Orleans, Louisiana, USA, 25–28 September. SPE-28550-MS. https://doi.org/10.2118/28550-MS.

Kuehne, D. L., Ehman, D. I., Emanuel, A. S. et al. 1990. Design and Evaluation of a Nitrogen-Foam Field Trial. J Pet $Technol$ 42 (2): 504–512. SPE-17381-PA. https://doi.org/10.2118/17381-PA.

Lake, L. W., Johns, R. T., Rossen, W. R. et al. 2014. $Fundamentals$ of $Enhanced$ Oil $Recovery$. Richardson, Texas, USA: Society of Petroleum Engineers.

Martinsen, H. A. and Vassenden, F. 1999. Foam-Assisted Water Alternating Gas (FAWAG) Process on Snorre. Paper presented at the European IOR Symposium, Brighton, UK, 18–20 August. https://doi.org/10.3997/2214-4609.201406335.

Matthews, C. S. 1989. Carbon Dioxide Flooding. In $Developments$ in $Petroleum$ $Science$, ed. E. C. Donaldson, G. V. Chilingarian, and T. F. Yen, Chap. 6, 129–156. Amsterdam, The Netherlands: Elsevier.

Morphy, P. H., Greenwald, K. G., and Herries, P. E. 1998. Operational Experience with Foam-Diverted Acid Jobs in the Gulf of Mexico. Paper presented at the SPE Formation Damage Control Conference, Lafayette, Louisiana, USA, 18–19 February. SPE-39423-MS. https://doi.org/10.2118/39423-MS.

Mukherjee, J., Nguyen, Q. P., Scherlin, J. M. et al. 2016. CO_2 Foam Pilot in Salt Creek Field, Natrona County, WY: Phase III: Analysis of Pilot Performance. Paper presented at the SPE Improved Oil Recovery Conference, Tulsa, Oklahoma, USA, 11–13 April. SPE-179635-MS. https://doi.org/10.2118/179635-MS.

Nguyen, Q. P., Currie, P. K., and Zitha, P. L. J. 2003. Determination of Foam Induced Fluid Partitioning in Porous Media using X-Ray Computed Tomography. Paper presented at the International Symposium on Oilfield Chemistry, Houston, Texas, USA, 5–7 February. SPE-80245-MS. https://doi.org/10.2118/80245-MS.

Nguyen, Q. P., Zitha, P. L. J., Currie, P. K. et al. 2009. CT Study of Liquid Diversion with Foam. SPE $Prod$ $&$ $Oper$ 24 (1): 12–21. SPE-93949-PA. https://doi.org/10.2118/93949-PA.

Norris, S. O., Scherlin, J. M., Mukherjee, J. et al. 2014. CO_2 Foam Pilot in Salt Creek Field, Natrona County, WY: Phase II: Diagnostic Testing and Initial Results. Paper presented at the SPE Annual Technical Conference and Exhibition, Amsterdam, The Netherlands, 27–29 October. SPE-170729-MS. https://doi.org/10.2118/170729-MS.

O'Sullivan, T. D. and Smith, N. 1970. The Solubility and Partial Molar Volume of Nitrogen and Methane in Water and in Aqueous Sodium Chloride from 50 to 125° and 100 to 600 atm. J $Phys$ $Chem$ 74 (7): 1460–1666. https://doi.org/10.1021/j100702a012.

Ransohoff, T. C. and Radke, C. J. 1988. Mechanisms of Foam Generation in Glass-Bead Packs. SPE Res $Eval$ $&$ Eng 3 (2): 573–585. SPE-15441-PA. https://doi.org/10.2118/15441-PA.

Rossen, W. R. 1996. Foams in Enhanced Oil Recovery. In $Foams:$ $Theory,$ $Measurements$ and $Applications$, ed. R. K. Prud'homme and S. A. Khan, Chap. 11, 413–464. New York, New York, USA: Marcel Dekker.

Rossen, W. R., Ocampo-Florez, A. A., Restrepo, A. et al. 2014. Long-Time Diversion in SAG Foam Enhanced Oil Recovery from Field Data. Paper presented at the SPE Annual Technical Conference and Exhibition, Amsterdam, The Netherlands, 27–29 October. SPE-170809-MS. https://doi.org/10.2118/170809-MS.

Rossen, W. R. and Renkema, W. J. 2007. Success of Foam SAG Process in Heterogeneous Reservoirs. Paper presented at the SPE Annual Technical Conference and Exhibition, Anaheim, California, USA, 11–14 November. SPE-110408-MS. https://doi.org/10.2118/110408-MS.

Rossen, W. R., van Duijn, C. J., Nguyen, Q. P. et al. 2010. Injection Strategies to Overcome Gravity Segregation in Simultaneous Gas and Water Injection into Homogeneous Reservoirs. SPE $J.$ 15 (1): 76–90. SPE-99794-PA. https://doi.org/10.2118/99794-PA.

Schindelin, J., Arganda-Carreras, I., Frise, E. et al. 2012. Fiji: An Open-Source Platform for Biological-Image Analysis. Nat $Methods$ 9 (7): 676–682. https://doi.org/10.1038/nmeth.2019.

Schramm, L. L. 1994. $Foams:$ $Fundamentals$ and $Applications$ in the $Petroleum$ $Industry.$ $Advances$ in $Chemistry$, Vol. 242. Washington, DC, USA: American Chemical Society.

Shan, D. and Rossen, W. R. 2004. Optimal Injection Strategies for Foam IOR. SPE $J.$ 9 (2): 132–150. SPE-88811-PA. https://doi.org/10.2118/88811-PA.

Shi, J. and Rossen, W. R. 1998. Improved Surfactant-Alternating-Gas Foam Process to Control Gravity Override. Paper presented at the SPE/DOE Improved Oil Recovery Symposium, Tulsa, Oklahoma, USA, 19–22 April. SPE-39653-MS. https://doi.org/10.2118/39653-MS.

Skauge, A., Aarra, M. G., Surguchev, L. et al. 2002. Foam-Assisted WAG: Experience from Snorre Field. Paper presented at the SPE/DOE Improved Oil Recovery Symposium, Tulsa, Oklahoma, USA, 13–17 April. SPE-75157-MS. https://doi.org/10.2118/75157-MS.

Talabani, S. and Islam, M. R. 1999. Diverting Acid into Low Permeability Reservoir Using Foam for Stimulation. Paper presented at the Technical Meeting/Petroleum Conference of the South Saskatchewan Section, Regina, Canada, 18–21 October. PETSOC-99-122. https://doi.org/10.2118/99-122.

Thompson, K. E. and Gdanski, R. D. 1993. Laboratory Study Provides Guidelines for Diverting Acid with Foam. SPE $Prod$ $&$ Fac 8 (4): 285–290. SPE-23436-PA. https://doi.org/10.2118/23436-PA.

Wang, S. and Mulligan, C. N. 2004. An Evaluation of Surfactant Foam Technology in Remediation of Contaminated Soil. $Chemosphere$ 57 (9): 1079–1089. https://doi.org/10.1016/j.chemosphere.2004.08.019.

Zeilinger, S. C., Wang, M., Kibodeaux, K. R. et al. 1995. Improved Prediction of Foam Diversion in Matrix Acidization. Paper presented at the SPE Production Operations Symposium, Oklahoma City, Oklahoma, USA, 2–4 April. SPE-29529-MS. https://doi.org/10.2118/29529-MS.

Jiakun Gong is a post-doctoral degree researcher at Delft University of Technology, The Netherlands. His current research interests include flow in naturally fractured reservoirs, foam EOR, and gas trapping. Gong holds a PhD degree from Delft University of Technology.

Sebastien Vincent-Bonnieu is reservoir engineer at Shell Global Solutions International. He is also a researcher at Delft University of Technology. His current research interests include gas/chemical EOR and carbon capture, utilization, and storage.

Ridhwan Zhafri Kamarul Bahrim is a petroleum engineer, specializing in reservoir engineering, in the research and development (R&D) division of the Malaysian national oil company, Petronas. He has been involved as a reservoir technologist in various projects that cover the aspects of production enhancement, EOR, field development planning, and EOR pilot implementations in Peninsular and East Malaysia. He also works with Shell through joint R&D, to find the best solutions for field rejuvenations and facility improvements. Kamarul Bahrim holds a degree in petroleum engineering from the Colorado School of Mines. He is also a member of SPE.

Che Abdul Nasser Bakri Che Mamat is currently working as the staff reservoir technologist at Petronas. He has in-depth technical knowledge and capability in evaluating petroleum fluid analysis (pressure/volume/temperature), chemical (foam, polymer, surfactant), and thermal (light oil air injection) EOR processes for Petronas' local and international assets. He was involved in the planning and execution of well-intervention programs using coiled tubing before joining Petronas. His main interests include laboratory analysis, reservoir simulation, and pilot implementation of EOR processes.

Raj Deo Tewari is a custodian and group technical authority in reservoir engineering at Petronas. He is involved with EOR research at Petronas, is an industry adviser to University Technology Petronas, and serves as chairman of technology research at Petronas. His main interests include field development planning, reservoir management and surveillance, and EOR. He is a recipient of the 2015 SPE Asia Pacific Technical Award.

Mohammad Iqbal Mahamad Amir is a petroleum engineer, specializing in reservoir engineering, in the R&D division of the Malaysian national oil company, Petronas.

Jeroen Groenenboom is the manager for chemical EOR technology for Shell at its Amsterdam Technology Centre. He worked in various locations for Shell (The Netherlands, Russia, Qatar, Malaysia, and China) in various roles in upstream development since 2001. Groenenboom holds an MSc degree in geophysics from Utrecht University and a PhD degree (cum laude) in hydraulic fracture monitoring from Delft University.

Rouhi Farajzadeh is a reservoir engineer for Shell. He is also a part-time assistant professor at Delft University of Technology and an adjunct professor at Rice University. He holds MS (cum laude) and PhD (cum laude) degrees in reservoir engineering, both from Delft University of Technology, and he holds a BS degree in chemical engineering from Tehran Polytechnic. He is an executive editor for *Journal of Petroleum Science and Engineering* and serves as a technical reviewer for SPE journals. He is the recipient of the 2018 SPE North Sea Regional Reservoir Description and Dynamics Award.

William Rossen is a professor of reservoir engineering in the Department of Geoscience and Engineering at Delft University of Technology. His current research concerns using foams for diverting fluid flow in porous media, modeling complex transport processes in networks, and understanding flow in naturally fractured geological formations. He received recognition as Best Instructor at Delft University of Technology in 2011 and received the 2012 IOR Pioneer Award. He is an SPE Distinguished Member.